Experimental study of Brillouin scattering in fluorine-doped single-mode optical fibers

Weiwen Zou,* Zuyuan He, and Kazuo Hotate

Department of Electronic Engineering, The University of Tokyo, Tokyo 113-8656, Japan
*Corresponding author: zou@sagnac.t.u-tokyo.ac.jp

Abstract: We experimentally investigate Brillouin scattering properties in fluorine-doped single-mode optical fibers. The effective acoustic velocities determined from the measured dependences of acoustic resonance frequencies on optical wavelength are approximately equal to the individual acoustic velocities in the core and/or cladding regions. Brillouin gain coefficients are experimentally characterized and compared with that in a standard GeO_2-doped single-mode fiber. The result indicates that the acousto-optic coupling efficiencies in all fibers are almost 100 %, which means that Brillouin threshold value can not be simply increased by fluorine doping. Moreover, it is found that the dependences of acoustic resonance frequencies on applied strain or temperature change are quantitatively enhanced by fluorine dopants, which is in opposite trend when compared with germanium ones.

© 2008 Optical Society of America

OCIS codes: (190.4370) Nonlinear optics, fibers; (290.5830) Scattering, Brillouin; (060.2290) Fiber materials; (060.2310) Fiber optics; (060.2270) Fiber characterization.

References and links

1. G. P. Agrawal, *Nonlinear Fiber Optics*, (Academic Press, 3rd version, 2001).
2. A. Kobyakov, S. Kumar, D. Q. Chowdhury, A. B. Ruffin, M. Sauer, and S. R. Bickham, "Design concept for optical fibers with enhanced SBS threshold," Opt. Express **13**, 5338–5346 (2005).
3. W. Zou, Z. He, and K. Hotate, "Acoustic modal analysis and control in w-shaped triple-layer optical fibers with highly-germanium-doped core and F-doped inner cladding," Opt. Express **16**, 10006–10017 (2008).
4. M. Nikles, L. Thevenaz, P. A. Robert, "Simple distributed fiber sensor based on Brillouin gain spectrum analysis," Opt. Lett. **21**, 738–740 (1996).
5. K. Hotate and M. Tanaka, "Distributed fiber Brillouin strain sensing with 1-cm spatial resolution by correlation-based continuous-wave technique," IEEE Photon. Technol. Lett. **14**, 179–181 (2002).
6. Y. Okawachi, M. S. Bigelow, J. E. Sharping, Z. Zhu, A. Schweinsberg, D. J. Gauthier, R. W. Boyd, and A. L. Gaeta, "Tunable all-optical delays via Brillouin slow light in an optical fiber," Phys. Rev. Lett. **94**, 153902 (2005).
7. K. Y. Song, M. G. Herraez, and L. Thevenaz, "Observation of pulse delaying and advancement in optical fibers using stimulated Brillouin scattering," Opt. Express **13**, 82–88 (2005).
8. Z. Zhu, D. J. Gauthier, and R. W. Boyd, "Stored light in an optical fiber via stimulated Brillouin scattering," Science **318**, 1748–1750 (2007).
9. T. Sugie, "Transmission limitation of CPFSK coherent lightwave systems due to stimulated Brillouin scattering in optical fiber," J. Lightwave Technol. **9**, 1145–1155 (1991).
10. A. Wada, T. Nozawa, D. Tanaka, T. Sakai, and R. Yamauchi, "Suppression of stimulated Brillouin scattering by intentionally induced periodical residual-strain in single-mode optical fibers," IEICE Trans. Commun. **E76-B**, 345–351 (1993).
11. J. Hansryd, F. Dross, M. Westlund, P. A. Andrekson, and S. N. Knudsen, "Increase of the SBS threshold in a short highly nonlinear fiber by applying a temperature distribution," J. Lightwave Technol. **19**, 1691–1697 (2001).

12. W. Zou, Z. He, A. D. Yablon, and K. Hotate, "Dependence of Brillouin frequency shift in optical fibers on draw-induced residual elastic and inelastic strains," IEEE Photon. Technol. Lett. **19**, 1389–1391 (2007).

13. J. Yu, I. Kwon, and K. Oh, "Analysis of Brillouin frequency shift and longitudinal acoustic wave in a silica optical fiber with a triple-layered structure," J. Lightwave Technol. **21**, 1779–1786 (2003).

14. K. Shiraki, M. Ohashi, and M. Tateda, "SBS threshold of a fiber with a Brillouin frequency shift distribution," J. Lightwave Technol. **14**, 50–57 (1996).

15. P. D. Dragic, C. H. Liu, G. C. Papen, and A. Galvanauskas, "Optical fiber with an acoustic guiding layer for stimulated Brillouin scattering suppression," in *CLEO'2005*, paper CThZ3, 2005.

16. T. Nakanishi, M. Tanaka, T. Hasegawa, M. Hirano, T. Okuno, and M. Onishi, "Al_2O_3-SiO_2 core highly nonlinear dispersion-shifted fiber with Brillouin gain suppression improved by 6.1 dB", in *ECOC'2006*, post-deadline paper Th. 4.2.2, 2006.

17. M. J. Li, X. Chen, J. Wang, S. Gray, A. Liu, J. A. Demeritt, A. B. Ruffin, A. M. Crowley, D. T. Walton, and L. A. Zenteno, "Al/Ge co-doped large mode area fiber with high SBS threshold," Opt. Express **15**, 8290–8299 (2007).

18. C. K. Jen, C. Neron, A. Shang, K. Abe, L. Bonnell, and J. Kushibiki, "Acoustic characterization of silica glasses," J. Am. Ceram. Soc. **76**, 712–716 (1993).

19. D. A. Pinnow, T. C. Rich, F. W. Ostermayer, and M. DiDomenico, "Fundamental optical attenuation limits in the liquid and glassy state with application to fiber optical waveguide materials," Appl. Phys. Lett. **22**, 527–529, 1983.

20. W. Zou, Z. He, M. Kishi, and K. Hotate, "Stimulated Brillouin scattering and its dependences on temperature and strain in a high-delta optical fiber with F-doped depressed inner cladding," Opt. Lett. **32**, 600–602 (2007).

21. N. Shibata, K. Okamoto, and Y. Azuma, "Longitudinal acoustic modes and Brillouin-gain spectra for GeO_2-doped-core single-mode fibers," J. Opt. Soc. Am. B **6**, 1167–1174 (1989).

22. M. Nikles, L. Thevenaz, and P. A. Robert, "Brillouin gain spectrum characterization in single-mode optical fibers," J. Lightwave Technol. **15**, 1842–1851 (1997).

23. A. L. Gaeta and R.W. Boyd, "Stochastic dynamics of stimulated Brillouin scattering in an optical fiber," Phys. Rev. A **44**, pp. 3205-3209, 2002.

24. W. Zou, Z. He, and K. Hotate, "Two-dimensional finite element modal analysis of Brillouin gain spectra in optical fibers," IEEE Photon. Technol. Lett. **18**, 2487–2489 (2006).

25. T. Mito, S. Fujino, H. Takeba, K. Morinaga, S. Todoroki, and S. Sakaguchi, "Refractive index and material dispersions of multi-component oxide glasses," J. Non-Cryst. Solid. **210**, 155–162 (1997).

26. Y. Koyamada, S. Sato, S. Nakamura, H. Sotobayashi, and W. Chujo, "Simulating and designing Brillouin gain spectrum in single-mode fibers," J. Lightwave Technol. **22**, 631–639 (2004).

27. W. Zou, Z. He, and K. Hotate, "Investigation of strain- and temperature-dependences of Brillouin frequency shifts in GeO_2-doped optical fibers," J. Lightwave Technol. **26**, 1854–1861 (2008).

1. Introduction

It is well known that stimulated Brillouin scattering (SBS) in silica-based optical fibers happens at a lower power level (threshold value) than other nonlinear effects such as stimulated Raman scattering. This is because Brillouin gain coefficient is higher by two orders of magnitude than Raman gain coefficient [1], and the coupling between the optical wave and the light-generated acoustic wave is efficient [2]. Especially, an acousto-optic coupling efficiency of about 100 % occurs in GeO_2-doped single-mode optical fibers (SMF) since the acoustic velocity in the core is reduced when compared with that in the pure-silica cladding and thus the acoustic wave is efficiently guided in the GeO_2-doped core even better than done the optical wave [3]. The SBS properties of the low threshold value together with the narrow resonance width and the long lifetime of the acoustic wave provide fruitful applications, such as fiber-optic distributed sensing [4, 5], all-optical slow-light control [6, 7], and a novel optical storage [8]. On the other hand, the low Brillouin threshold value is one of the most dominant factors to influence the optical fiber communications since the optical light is exponentially backscattered if the light power exceeds the threshold value. To overcome the power limitation, several different proposals have been demonstrated. One proposal was to apply frequency modulation or phase modulation to optical lights in order to broaden the Brillouin resonance linewidth and thus lower the overall Brillouin efficiency [9]. The second proposal was to modify the intrinsic Brillouin gain spectrum of optical fibers. Efforts have been artificially made by introducing draw-induced or temperature-induced residual stresses along the fiber's axial direction [10, 11].

This is because the residual stresses can modify the Brillouin frequency shift [12, 13] and thus weaken the whole-length Brillouin efficiency [14].

Recently, some novel efforts were made to increase the acousto-optic effective area A_{eff}^{ao} or lower the acousto-optic coupling efficiency $I_{ao} = A_{eff}/A_{eff}^{ao}$ with A_{eff} the optical effective area, and consequently enhance the SBS threshold value. Kobyakov *et al.* [2] demonstrated one method to modify the optical refractive index and thus weaken the acousto-optic coupling efficiency. In [15, 16, 17], a new design concept was proposed by use of some silica dopants (such as Al-doped silica or co-doped silica by Al and other dopants). This concept was based on the previous finding by Jen *et al.* [18] that various silica dopants could provide the opposite performances to the optical guiding and the acoustic guiding. It was reported that the acousto-optic effective area A_{eff}^{ao} and the SBS threshold could be increased to some extent (such as $\sim$6dB) [15, 16, 17]. Fluorine-doped silica possesses a smaller refractive index than pure silica so that it has been used as a cladding material to fabricate pure-silica-core optical fibers with a lower optical loss than GeO_2-doped optical fibers [19]. Because fluorine-doped silica reduces the acoustic velocity [18], the acoustic guiding property in fluorine-doped optical fibers should be reversed according to the design concept given in [15, 16, 17], and then the SBS threshold value should be increased in principle.

This paper presents our experimental investigation of the SBS properties in fluorine-doped single-mode optical fibers (F-SMFs). The fibers are composed of one with pure-silica core and the other with fluorine-doped-silica core, both with fluorine-doped-silica claddings. Our study shows that the acousto-optic coupling efficiencies in the F-SMFs are the same as that in a standard GeO_2-doped SMF (i.e., 100 %). In other words, SBS threshold value cannot be increased simply by fluorine doping. Moreover, we study, for the first time to our best knowledge, the dependences of the SBS in the F-SMFs on strain and temperature, which is meaningful for the study on Brillouin-based discriminative sensing of strain and temperature [20, 3]. It is found that the strain and temperature sensitivities of acoustic resonance frequencies are enhanced if the fluorine concentration is increased, which is opposite to the germanium doping.

2. SBS key properties

Brillouin gain spectrum (BGS) in a single-mode optical fiber (either GeO_2-doped or fluorine-doped one) could experience multiple resonance peaks. The peaks arise from multiple longitudinal acoustic modes that exist in the fiber's core and/or the fiber's cladding [21]. The acoustic resonance frequency (ν_i) is defined by

$$\nu_i = (2n_{eff}V_a^i) \cdot \lambda_o^{-1}, \tag{1}$$

where V_a^i is the effective acoustic velocity of ith-order resonance acoustic mode, n_{eff} is the effective modal refractive index, and λ_o is the optical frequency in vacuum.

The main-peak gain coefficient (g_{B0}) of the fundamental acoustic resonance mode in the fiber's core at the main-peak resonance frequency (i.e., Brillouin frequency shift, BFS, ν_{BFS}) is determined by

$$g_{B0} = \frac{2\pi p_{12}^2}{c\lambda_o^2 \rho_0} \cdot \frac{n_{eff}^7}{V_a^{BFS}} \cdot \frac{1}{\Delta\nu_{BFS}}, \tag{2}$$

where ρ_0 is the material density and p_{12} is the photo-elastic constant that have no significant difference in silica-based materials; c is the light speed in vacuum; V_a^{BFS} is the effective acoustic velocity of the fundamental acoustic resonance mode and $\Delta\nu_{BFS}$ is the Brillouin main-peak linewidth of the fundamental acoustic mode.

It was reported that the Brillouin main-peak linewidth ($\Delta\nu_{BFS}$) of the fundamental acoustic mode has a significant difference between GeO_2-doped silica and fluorine-doped silica [22].
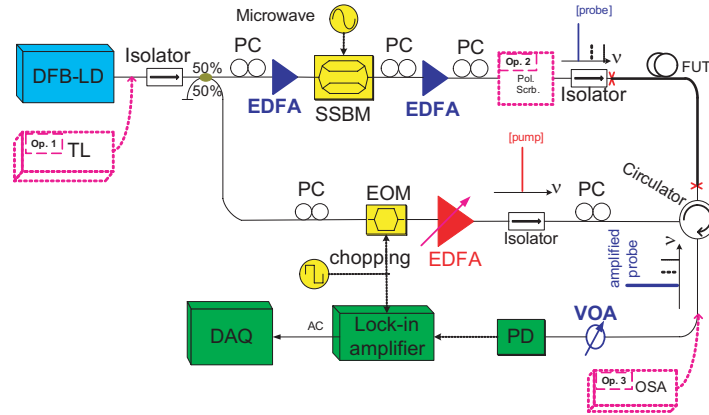
Fig. 1. Experimental setup of SBS-based measurement system. DFB-LD, distributed-feedback laser diode; SSBM, single-sideband modulator; EOM, electro-optic modulator; EDFAs, erbium-doped fiber amplifiers; PCs, polarization controllers; VOA, variable optical attenuator; PD, photo-detector; DAQ, data acquisition card; FUT, fiber under test; TL, tunable laser; Pol. Scrb., polarization scrambler; OSA, optical spectrum analyzer.

Meanwhile, the main-peak $\Delta\nu_{BFS}$ in the GeO_2-doped-core fiber is known as a function of Brillouin single-pass gain (G_s)

$$G_s = \frac{g_{B0}P_pL_{eff}}{A_{eff}^{ao}K},$$

(3)

as follows [23]:

$$\Delta\nu_{BFS} = \Delta\nu_{B0}(\frac{ln2}{G_s})^{1/2},$$

(4)

where $L_{eff} = [1 - exp(-\alpha L)]/\alpha$ is the effective length of the fiber with α the optical loss and L the fiber length, P_p is the pump power (in [mW]), K is a polarization factor (= 2 for a complete polarization scrambling process) and $\Delta\nu_{B0}$ means the intrinsic linewidth determined by the phonons' damping rate. Note that the above equation (4) is not suitable for the SBS process with significant depletion of pump power. The Brillouin exponential amplification of the probe power (P_{probe}) is expressed by

$$G_e \equiv \frac{\Delta P_{probe}}{P_{probe}} = exp\{G_s\}.$$

(5)

3. Experimental setup

The experimental setup to investigate the SBS properties is based on a pump-probe scheme as depicted in Fig. 1. The major part of the scheme has been explained in Ref. [20]. To study the acoustic resonance frequencies dependence on optical wavelength (λ_o), a 1525∼1575-nm tunable laser (TL, HP 81689A, see dashed box "Op1" in Fig. 1) is employed. For all other characterizations, a distributed-feedback laser diode (DFB-LD) with a 3-dB linewidth of about 2 MHz is used as a light source.

To measure the Brillouin gain coefficients, a polarization scrambler (Pol. Scrb., FIBERPRO PS3000, see dashed box "Op.2" in Fig. 1) is firstly introduced to scramble the polarization state of the Brillouin probe signal. Second, an optical spectrum analyzer (OSA, Advantest Q8384, see dashed box "Op.3" in Fig. 1) with a spectral resolution of 0.01 nm is used to detect the amplified power of the probe signal, whose central optical frequency is down-shifted from the

Table 1. Parameter list of fiber samples

Fiber Sample	SMF	F-SMF-1	F-SMF-2
Core	GeO_2-doped silica	Pure silica	F-doped silica
Cladding	Pure silica	F-doped silica	F-doped silica
Δ (%) *	0.36, 0	0, -0.42	-0.30, -0.60
α (dB/km)	0.21	0.18	0.31
Length (m)	180	50	110
L_{eff}(m)	179.2	49.9	109.6
MFD (μm)	10.41	9.60	11.11
n_{eff}**	1.446	1.441	1.437
A_{eff}**(μm^2)	79	76	97

*Corresponding to core and cladding, respectively.

**Calculated by finite element method.

pump signal by just the Brillouin frequency shift (BFS) via a microwave synthesizer and a single-sideband modulator (SSBM).

Three fiber samples are tested: a standard GeO_2-doped-core SMF, F-SMF-1 with pure-silica core and fluorine-doped-silica cladding, and F-SMF-2 with lower-fluorine-doped-silica core and higher-fluorine-doped-silica cladding. All the fiber samples are only coated with a 250-μm polymer jacket. The modeled refractive index profiles provided by Fujikura Ltd. are approximately step-like and summarized in Table 1, in which the modeled relative refractive index is defined as

$$\Delta \equiv (n_1 - n_0)/n_0 \times 100\%, \qquad (6)$$

where n_1 is the refractive index of the modeled region and n_0 is the refractive index of pure silica as a referece. The optical loss coefficient α and the modal field diameter (MFD) are measured at 1.55-μm region. The effective refractive indices (n_{eff}) and the A_{eff} at 1.55-μm region are numerically calculated upon the modeled refractive index profiles by using the finite element method [3, 24] and setting the refractive index of pure silica (n_0 = 1.444) [25].

To measure the strain dependence, each ∼10-m fiber under test (FUT) is maintained at room temperature whereas different axial strains are applied upon the FUT. To measure the temperature dependence, the FUT is laid in the loose state free of strain while its temperature is altered within an accuracy of 0.1-^{o}C.

4. Experimental results

4.1. SBS properties

Figure 2(a) shows the measured BGS of the F-SMFs when an axial strain is not applied or applied upon the FUT, for which the light source is 1.549-μm DFB-LD and the pump (probe) power measured after the optical circulator (isolator) is ∼21.8 dBm (∼-1.0 dBm). From Fig. 2(a), we can see that there are two peaks (b and c) in F-SMF-2, both of which are moved when the strain is applied. However, only one peak (a) in F-SMF-1 is moved while the other weak peak does not shift with the applied strain. A possible reason is that the weak peak is located close to that of SMF pigtails (∼15 cm) spliced to the F-SMF-1, but no strain was applied on the SMF pigtails. Table 2 summarizes those acoustic resonance frequencies (ν_i) at 1.549 μm and the corresponding linewidths ($\Delta\nu_i$) where i = a, b or c denotes the peak a, b or c, respectively.

According to Fig. 2(b), where ν_i are measured under different optical wavelength λ_o with the 1525∼1575-nm TL as the light source, we can evaluate the respective V_a via Eq. (1) for peak a, b or c, respectively, as listed in Table 2. The fluorine concentrations ([F], in unit of $wt\%$) in the
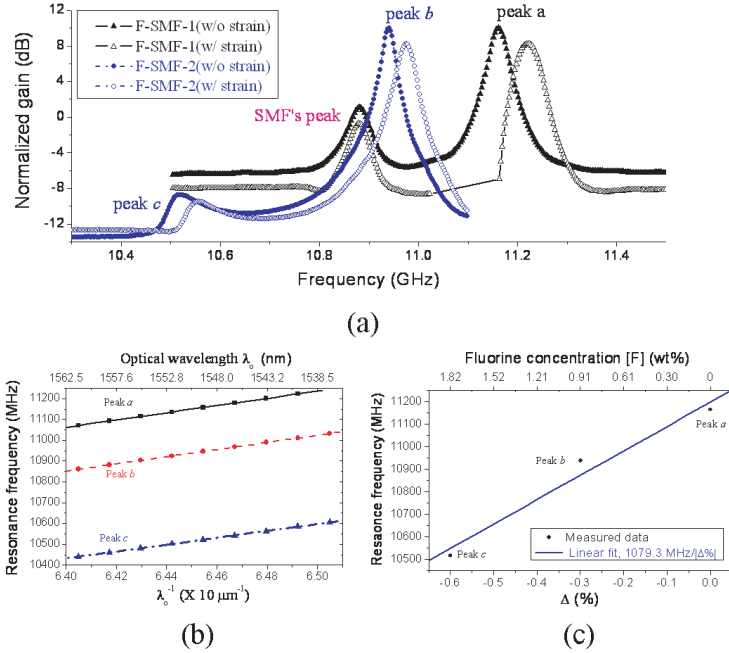
Fig. 2. (a) Measured BGS of F-SMF-1 and F-SMF-2 without or with strain applied, respectively. (b) Acoustic resonance frequencies of peaks *a*, *b* and *c*, respectively, as functions of optical wavelength λ_o. Symbolic points, measured results; solid line, linear fitting. (c) Acoustic resonance frequencies of peaks *a*, *b* and *c* measured at 1.549 μm as a function of the relative refractive index (Δ). Circles, measured results; solid line, linear fitting.

Table 2. Summary of measured and deduced parameters of peaks *a*, *b* and *c*

Fiber Sample	F-SMF-1	F-SMF-2	
Peaks	*a*	*b*	*c*
ν_i (MHz)	11165.2	10939.7	10517.6
$\Delta\nu_i$ (MHz)	~27	~28	~115
n_{eff}	1.441	1.437	1.437
$d\nu_i/d\lambda_o^{-1}$ (10^4 m/s)	1.728	1.712	1.657
V_a (m/s)	5996	5898	5672
Δ (%)	0	-0.30	-0.60
[F] (wt%)*	0	0.91	1.82
V_l^*	5944	5798	5652

*Deduced from the modeled Δ.

F-SMFs' core and cladding regions are deduced from the modeled refractive indices as [F] = $|\Delta|/0.33\%$, and then the corresponding longitudinal acoustic velocities are calculated according to $V_l = V_{l0}(1 - 2.7 \times 10^{-2}[\text{F}])$ with V_{l0}=5944 m/s the acoustic velocity of pure silica [26]. All of V_a, [F] and V_l are summarized in Table 2. Compared with the acoustic velocities (V_l) decided by fluorine concentration, the deduced effective acoustic velocities (V_a) qualitatively confirm that the peak *a* dominantly locates in the pure-silica core of F-SMF-1, and the peak *b* dominantly exists in the fluorine-doped core while the peak *c* in the fluorine-doped cladding of F-SMF-2.
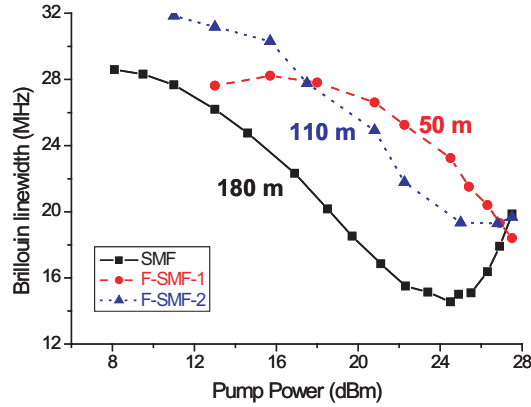
Fig. 3. Measured Brillouin linewidth in F-SMFs and SMF varying with the increased Brillouin pump power.

Moreover, the acoustic resonance frequencies (v_i) of F-SMFs measured at 1.549 μm are plotted in Fig. 2(c) as a function of the relative refractive index (Δ) showing a linear dependence while a little non-monotonically. Linear fitting to data gives a linear slope of 1079.3 MHz/Δ% meaning that the ~327.1-MHz resonance frequency is decreased by per wt% increase of fluorine concentration, which confirms the previously-reported result by Shibata *et al.* [21]. The finite deviation from the linear dependence is possibly attributed to the different residual stresses stored into the F-SMFs that can raise significant influence to the acoustic resonance frequency [12].

The narrowing phenomenon of the Brillouin main-peak linewidth (Δv_{BFS}) as estimated in Eq. (4) is observed in either SMF or F-SMFs when the pump power is intensified. For these measurements, 1.549-μm DFB-LD is used as the light source and the Brillouin probe power is ~-1 dBm with a peak power measured by the OSA as ~-22 dBm. The experimental results are plotted in Fig. 3. Considering the different L_{eff} of three fiber samples as listed in Table 1, we can predict that the Brillouin main-peak linewidths of F-SMFs are comparable to each other and also to that of SMF. This result is far different from the previously-reported in Ref. [22]. Furthermore, according to Eq. (2), this result shows that it is reasonable to assume that the main-peak gain coefficient (g_{B0}) is the same in those silica-based materials (i.e., GeO$_2$-doped, fluorine-doped or pure silica). When the pump power is intensified to a high value above ~24 dBm (~250 mW), the Brillouin main-peak linewidth of SMF becomes increasing. This reason is possibly that the pump power depletes much faster than its contribution to the single-pass gain G_s since the probe light experiences an amplification of more than 20 dB for a greater pump power than ~24 dBm, which will be described in Fig. 4. From the other point of view, during BGS measurement, the Brillouin probe light with a down-shifted frequency of just the BFS (v_{BFS}) feels more significantly the depletion of the pump power than the one with a down-shifted frequency of a finite offset from the v_{BFS}.

Figure 4(a) describes the measured amplification (in [dB]) to the Brillouin probe signal under different pump power (in [mW]) for the F-SMFs and SMF, which is defined by

$$G_{dB} = 10log_{10}(G_e). \tag{7}$$

During the measurement, the pump-probe frequency offset is fixed at the fiber's individual BFS, the amplified probe power is monitored through the OSA, and the probe's polarization state is completely scrambled. If the Pol. Scrb. is not introduced to the probe light, the measured BGS or the Brillouin amplification is not unique when the pump or probe light is set under
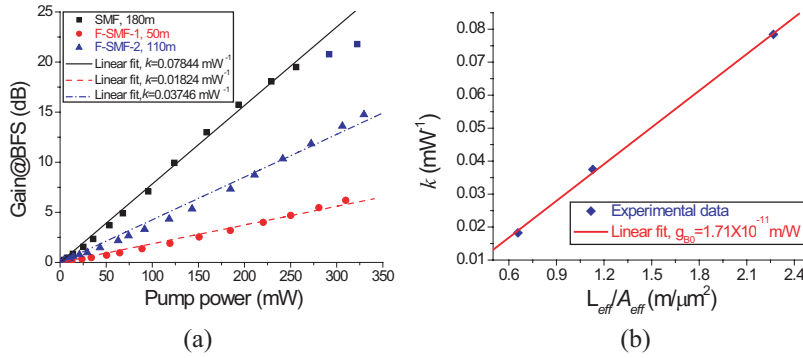
Fig. 4. (a) Measured Brillouin amplification to the Brillouin probe light under different Brillouin pump power for F-SMFs and SMF. The polarization state of the probe light is completely scrambled by a Pol. Scrb., and the amplified probe power is measured by an OSA. Symbolic symbols, experimental results; linear curves, least-squares linear fitting. (b) The fitted linear slope k as a function of L_{eff}/A_{eff}. Diamond points, experimental result; linear curve, least-squares linear fitting.

various polarization states via polarization controllers (PCs). In contrast, when the complete polarization-scrambling process is introduced to the probe light by the Pol. Scrb., the maximized Brillouin amplification is halved and the amplification is not sensitive to the polarization state of the pump light any more.

The least-squares linear fitting to the experimental results in Fig. 4(a) provides the amplification rate defined by $k = \delta G_{dB}/\delta P_p$ (in [mW^{-1}]), which can be deduced from Eqs. (3), (5) and (7) as:

$$k = \frac{10log_{10}(e)}{K} \cdot \frac{L_{eff}}{A_{eff}^{ao}} \cdot g_{B0}. \tag{8}$$

In Fig. 4(b), the obtained k is plotted as a function of L_{eff}/A_{eff} instead of L_{eff}/A_{eff}^{ao}. The result shows a good linear dependence with an evaluated g_{B0} of 1.71×10^{-11} m/W. The good linearity further indicates that the A_{eff}^{ao} should be equal to the A_{eff} for both F-SMFs as like the case of SMF. In other words, all the acousto-optic coupling efficiencies I_{ao} in three fibers should be unity (i.e., 100 %). These results prove that Brillouin threshold value can not be increased by fluorine doping, which is far different from the design concept demonstrated in [15, 16, 17].

4.2. Strain and temperature dependences

The acoustic resonance frequency of peak a of F-SMF-1 or those of peaks b or c of F-SMF-2 is measured under different strain and temperature, respectively. The results are illustrated in Fig. 5(a) and 5(b), respectively. The least-squares linear fittings give the strain coefficients ($A_i = \delta v_i/\delta \varepsilon$ in [MHz/$\mu\varepsilon$]) and temperature coefficients ($B_i = \delta v_i/\delta T$ in [MHz/^{o}C]). Furthermore, the normalized coefficients ($A_i' = A_i/v_i$ in [$10^{-6}/\mu\varepsilon$] and $B_i' = B_i/v_i$ in [$10^{-6}/^o$C]) are deduced respectively.

All the above results are summarized in Table 3. Since peaks a, b and c correspond to incremental fluorine concentrations as shown in Fig. 2 (c), the normalized strain or temperature coefficient of the acoustic resonance peaks shows a dependence on the fluorine concentration. From Table 3, we can know qualitatively that the sensitivities of the acoustic resonance frequencies to strain and/or temperature are enhanced if the fluorine concentration is increased. This trend is opposite to the case of germanium doping [27].
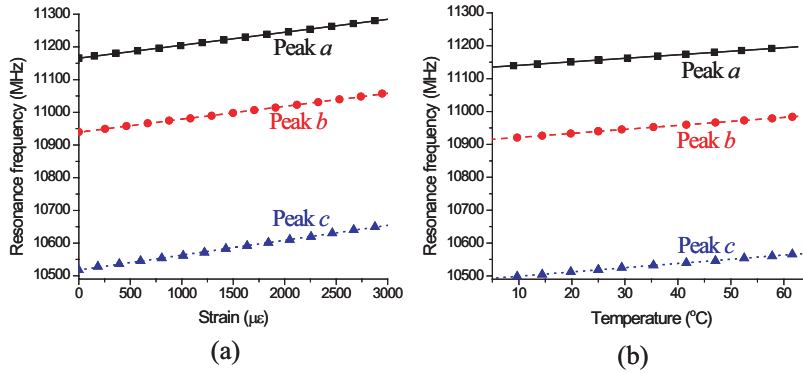
Fig. 5. (a) Strain and (b) temperature dependences of the acoustic resonance frequencies in both F-SMFs. Symbolic points, experimental results; linear curves, least-squares linear fitting.

Table 3. Strain and temperature coefficients of acoustic resonance frequencies in F-SMFs

Fiber Sample	F-SMF-1	F-SMF-2	
Peaks	a	b	c
Δ (%)	0	-0.30	-0.60
[F] (wt%)	0	0.91	1.82
A (MHz/$\mu\varepsilon$)	0.0396	0.0396	0.0456
A' (10^{-6}/$\mu\varepsilon$)	3.547	3.620	4.336
B (MHz/$^\circ$C)	1.075	1.211	1.286
B' (10^{-6}/$^\circ$C)	96.281	110.698	122.271

5. Conclusions

We have investigated experimentally the SBS and its dependences on strain and temperature in F-SMFs. The SBS property in F-SMFs has a great similarity to that in standard GeO_2-doped SMF although their acoustic guiding structures were thought different from each other. We proved that the Brillouin threshold value can not be increased simply by employing fluorine dopants, which is different from the expectation according to [15, 16, 17]. The characterized strain and temperature dependences show that the increase of fluorine concentration enhances the sensitivities of the acoustic resonance frequencies to strain and temperature, which is opposite to the case of GeO_2-doped silica.

6. Acknowledgment